Supplemental Material

A) Methods: Computer Modeling Supplement

Human Atrial Tissue Model

Membrane kinetics of the normal myocyte were represented by the Courtemanche-Ramirez-Nattel (CRN) model of the human atrial action potential.[1] Although several human atrial myocyte models exist,[1-3] only the CRN and the Nygren et al. models have been validated for use in both tissue[4-6] and organ[7-11] level simulations. We chose to use the CRN model over the Nygren et al. model for this study since it reproduces rate-dependent behaviors that closely matched the patient cohorts of this study. The mathematical formulation of the acetylcholine-activated potassium current ($I_{K(ACh)}$) from Kneller et al [12] was also included into the model to assess the effects of adenosine on membrane kinetics. Furthermore, we decreased the maximum conductance of I_{K1} by 20% to generate a baseline APD of 330 msec (to match patient APD, which is > 325 msec), since baseline APD in the tissue model was unrealistically short (290ms) when using the default parameters of the CRN model.

The human atrial tissue model, with the dimensions shown in Figure 6A of the manuscript, was discretized at a 100 μm resolution. Electrophysiological behavior at the tissue level was represented by the monodomain formulation. The tissue was assigned an isotropic conductivity value of 0.4 S/m to produce a conduction velocity of 62 cm/sec, which is well within the physiological range for normal conduction velocity in the atria.[10, 13]

Simulation of Atrial Fibrillation

Following Courtemanche et al,[14] modifications to ion current densities from protein remodeling during AF were simulated by reducing I_{CaL} by 70%, I_{to} by 50% and I_{Kur} by 50%. The

CRN model for AF[15] has been already validated for use in models from the single cell to the organ level.[9]

Simulation of Isoproterenol Effects

Beta-adrenergic stimulation from isoproterenol infusion was simulated by increasing the current densities of I_{CaL} by 300%,[16] I_{Kur} by 45%,[17] and I_{Ks} by 240%.[18] Alterations in I_{Kr} kinetics due to isoproterenol[19, 20] were simulated by factoring the forward and backward rate constants of the inactivation gating variable x_r by 3 and 1/3, respectively, to reduce I_{Kr} inactivation; these changes are within the range used in other modeling studies simulating beta-adrenergic stimulation.[21, 22] Since isoproterenol has also been shown to increase conductance through gap junctions, we increased the tissue conductivity in the model by 50% (from 0.4 S/m to 0.6 S/m).[23, 24]

Simulation of Adenosine Effects

Cholinergic stimulation from adenosine was simulated by increasing $I_{K(ACh)}$ by 123% and decreasing I_{CaL} by 12%,[25] then elevating acetylcholine concentration ([ACh]) until baseline APD shortened by at least 20 ms as observed clinically (Figure 4 and table S1 in the online supplement).

Pacing Protocol

Atrial tissue models were paced according to the clinical protocols. In summary, a drive train of 8 beats at a cycle length of 500 ms (S1) (baseline and adenosine) or 450 ms (isoproterenol) was followed by a single PAC (S2), coupled at 450, then 400, reduced in 20 ms

steps to 300, then in 10 ms steps to effective refractory period. In the rapid pacing simulation, pacing for 30 seconds was performed at CLs of 500, 450, then 400 msec, decrementing by 20 msec until 300 msec, then in 10 msec steps until loss of atrial capture.

Calculation of APD and Activation Latency Restitution

Model APD restitution curves were constructed in the same manner as for MAP data (outlined in the methods section "*Measurement of PAC-Related APD Restitution"* in the manuscript). APD restitution slope was determined for values within a 35 ms window beginning at the shortest diastolic interval. Model activation latency restitution curves were also constructed in the same manner as for MAP data (outlined in the methods section "*Analysis of Activation Latency – Rate Relationship"* in the manuscript). Importantly, activation latency in the model was defined as the time it takes for a wavefront to travel 0.5 cm away from the location of the stimulus (a product of conduction velocity) since tissue latency is not simulated in the atrial tissue monodomain model. Thus, the activation latency value computed in our tissue model is only a partial representation to activation latency recorded in patients. Future work will entail extending the tissue model to a more computationally expensive bidomain model with the ability to compute MAPs and tissue activation latency.

Simulation of the Effects of Rapid Pacing with Elevated $[K^+]_o$

The CRN model does not account for shortening of APD due to a rise in extracellular potassium concentration ($[K^+]_o$) during rapid pacing.[26, 27] Notably, pacing the AF model rapidly without extracellular potassium ($[K^+]_o$) accumulation did not steepen APD restitution slope (Figure 7A). So $[K^+]_o$ was increased by increments of 25% until APD restitution slope was >

1.0. Figure S2A illustrates the increase in APD restitution slope above 1.0 when local $[K^+]_o$ was increased by 75%, from 5.4 mmol/L to 9.45 mmol/L (which is within the concentrations used experimentally[28]). Once increased $[K^+]_o$ was factored into the model, the increase in APD restitution slope with rapid pacing was found to be due to increased I_{K1} density.

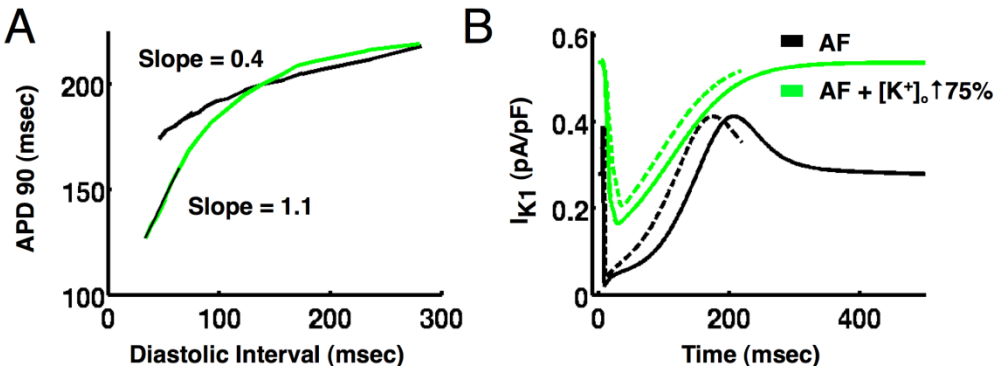

Figure S1. (A) APD restitution and **(B) I_{K1}** during rapid pacing in the baseline AF tissue model (black) and in the AF tissue model with elevated [K+]o (green). In panel B, solid lines represent steady-state I_{K1} at the pacing CL of 500 msec, while the dashed lines refer to steady-state I_{K1} at the pacing CL of 220 msec (the shortest CL before loss of atrial capture).

Determining the Mechanisms for APD and Activation Latency Restitution

To elucidate the role of ionic mechanisms in APD and activation latency restitution following pharmacological interventions, the contribution of each parameter modification representing the effect of isoproterenol and adenosine was determined by setting the value of the given parameter, one at a time, to its default AF value. Results are shown in manuscript figure 7C. Differences are the **inverse** of the contribution of each ionic current modification to the APD and AL restitution dynamics. The effect of each of these maneuvers on APD and activation latency restitution was then analyzed.

B) Results: Computer Modeling Supplement:

Data Used to Construct the Isoproterenol Plots in Figure 7C of the Manuscript

Figure S2A shows that when the increase in I_{CaL} is eliminated from the AF tissue model with isoproterenol, APD restitution slope significantly decreases more so than any other parameter modification, indicating that I_{CaL} is the major contributor to APD steepening with isoproterenol. Figure S2B shows that when decreased I_{Kr} inactivation is eliminated from the AF tissue model with isoproterenol, activation latency magnitude is significantly increased more so than any other parameter modification, indicating that I_{Kr} inactivation is the primary contributor to the reduced activation latency magnitude with isoproterenol.

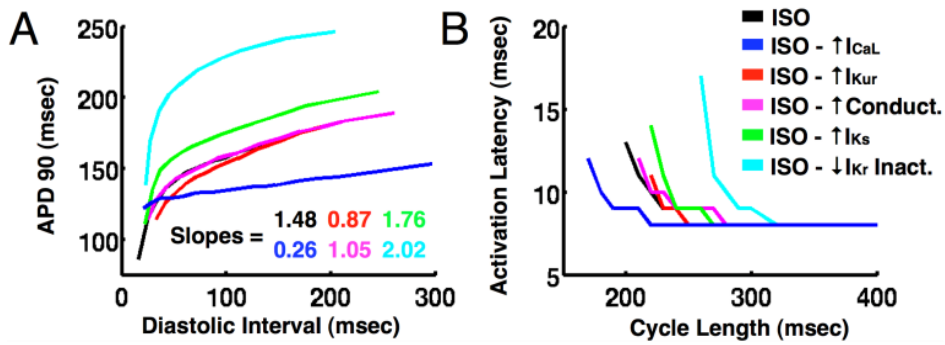

Figure S2. (A) APD and **(B) AL** restitution in the AF tissue model with isoproterenol, along with results from the simulations in which each parameter modification associated with isoproterenol infusion was set to its corresponding default AF value.

Data Used to Construct the Adenosine Plots in Figure 7C of the Manuscript

Figure S3A demonstrates that when the increases in [ACh] and $I_{K(ACh)}$ conductance are removed from the AF tissue model with adenosine, APD restitution slope flattens slightly, while removing the I_{CaL} reduction resulted in no change in APD restitution slope. This indicates that increased $I_{K(ACh)}$ via elevated [ACh] and enhanced conductance is responsible for the small increase in APD restitution slope (0.04) observed following adenosine infusion. Figure S3.B shows that activation latency magnitude decreases the most when [ACh] was removed from the AF tissue model with adenosine, indicating that elevated [ACh] plays a major role in increasing activation latency magnitude in the AF tissue model with adenosine.

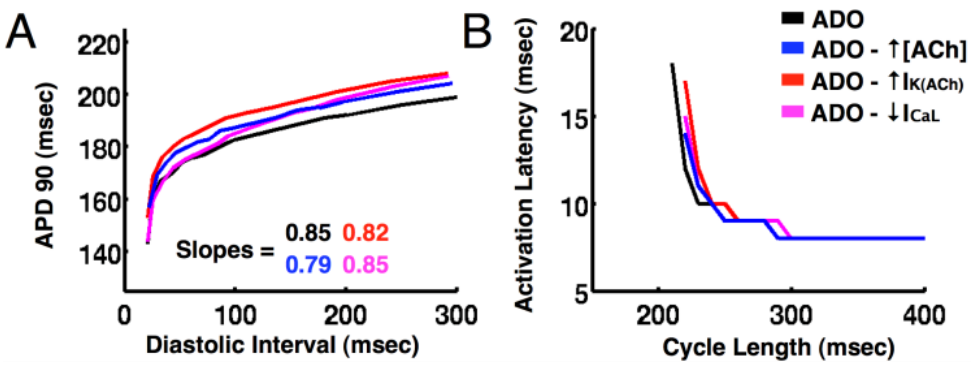

Figure S3. (A) APD and **(B) AL** restitution in the AF tissue model with adenosine, along with results from the simulations in which each parameter modification associated with adenosine infusion was set to its corresponding default AF value.

Ionic Currents for the AF Baseline, Isoproterenol, Adenosine and Rapid Pacing Simulations of Figure 2.A and 2.B in the Manuscript at Moderate and Fast Pacing Rates:

We calculated current traces during action potentials generated at long and at short diastolic intervals.

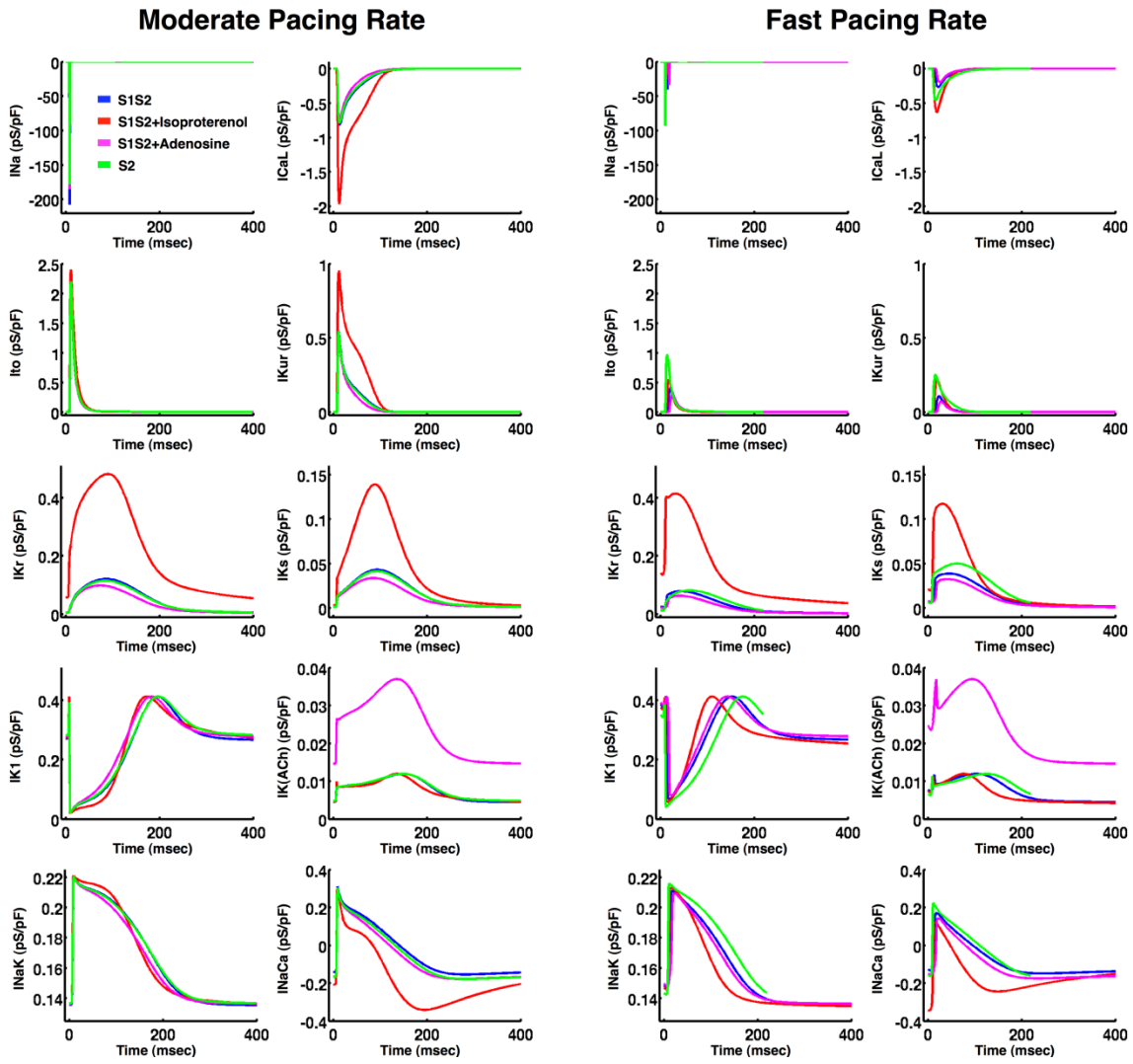

Figure S4. The ionic currents of the CRN model in the AF tissue model at baseline, and with isoproterenol, adenosine and rapid pacing for both moderate pacing (CL=400 msec) and fast pacing (shortest CL achieved; 230 msec for S1S2, 200 msec for S1S2+Isoproterenol, 210 msec for S1S2+Adenosine, and 220 msec for S2) rates.

C) Clinical Data Supplement

Table S1 shows the electrophysiologic properties of the study population of patients with atrial fibrillation at baseline and during each of the pro-arrhythmic interventions. As described in the statistical methods section, note that statistical comparisons between baseline and intervention were computed using the subset of the population for whom both baseline and intervention data were available using either the McNemar test (categorical data) or the paried *t*

test (continuous data). Thus, the reported mean and standard deviation for the comparison in the manuscript text may be slightly different than the overall group means, reported here.

Table S1. Left Atrial Electrophysiologic Properties of Patients with AF at Baseline and During Pro-Arrhythmic Interventions

EP Characteristic	S1S2 Baseline	S1S2 + Isoproterenol	S1S2 + Adenosine	Rapid Pacing
AF Induction, n (%)	5/43 (12%)	7/11 (64%)	1/10 (10%)	26/31 (84%)
Max ADPR slope	1.1±0.6	1.8±0.6	1.0±0.5	1.4±0.5
Min CL (ms)	257±25	203±12	205±13	218±32
Min DI (ms)	-14±18	-48±12	10±22	31±17
Min APD (ms)	196±39	154±32	145±30	132±21
Max AL (ms)	72±15	33±15	117±41	17±13

EP=electrophysiologic, AF=atrial fibrillation, APDR=action potential duration restitution, Min=minimum, CL=cycle length, ms=milliseconds, DI=diastolic interval, APD= action potential duration, AL=activation latency.

Table S2 shows the electrophysiologic properties of control patients (no history of atrial fibrillation) at baseline and during isoproterenol and rapid pacing. Adenosine was not infused in control patients.

Table S2. Left Atrial Electrophysiologic Properties of Control Patients at Baseline and During Pro-Arrhythmic Interventions

EP Properties	Baseline S1S2	Isoproterenol + S1S2	Rapid Pacing
APD Rest Slope	0.58±0.37	0.72±0.24	0.72±0.30
Min Cond CL (ms)	250±61	233±46	213±12
Min DI (ms)	**-17±13[a]**	**-25±33[b]**	**33±17[a,b]**
Min APD (ms)	258±58	220±43	173±32
Max AL (ms)	**64±17[a]**	**44±7[b]**	**17±3[a,b]**

Superscripts indicate $p<0.05$ for ([a]) baseline versus rapid pacing and ([b]) isoproterenol versus rapid pacing. EP=Electrophysiologic, Pts=patients, APD Rest=action potential duration restitution, Min=minimum, Cond=conducted, CL=cycle length, ms=milliseconds, DI=diastolic interval, AL=activation latency. For this table, statistics were calculated using repeated measures ANOVA with post hoc Bonferroni within each EP characteristic, using NCSS 2007 (Kaysville, UT, USA).

Online Data Supplement References

1. Courtemanche M, Ramirez RJ, Nattel S. Ionic mechanisms underlying human atrial action potential properties: Insights from a mathematical model. *Am J Physiol*. 1998;275:H301-321
2. Nygren A, Fiset C, Firek L, Clark JW, Lindblad DS, Clark RB, Giles WR. Mathematical model of an adult human atrial cell: The role of k+ currents in repolarization. *Circ Res*. 1998;82:63-81
3. Grandi E, Pandit SV, Voigt N, Workman AJ, Dobrev D, Jalife J, Bers DM. Human atrial action potential and ca2+ model: Sinus rhythm and chronic atrial fibrillation. *Circ Res*.109:1055-1066
4. Pandit SV, Berenfeld O, Anumonwo JM, Zaritski RM, Kneller J, Nattel S, Jalife J. Ionic determinants of functional reentry in a 2-d model of human atrial cells during simulated chronic atrial fibrillation. *Biophys J*. 2005;88:3806-3821
5. Atienza F, Almendral J, Moreno J, Vaidyanathan R, Talkachou A, Kalifa J, Arenal A, Villacastin JP, Torrecilla EG, Sanchez A, Ploutz-Snyder R, Jalife J, Berenfeld O. Activation of inward rectifier potassium channels accelerates atrial fibrillation in humans: Evidence for a reentrant mechanism. *Circulation*. 2006;114:2434-2442
6. Maleckar MM, Greenstein JL, Giles WR, Trayanova NA. K+ current changes account for the rate dependence of the action potential in the human atrial myocyte. *Am J Physiol Heart Circ Physiol*. 2009;297:H1398-1410
7. Jacquemet V, Virag N, Ihara Z, Dang L, Blanc O, Zozor S, Vesin JM, Kappenberger L, Henriquez C. Study of unipolar electrogram morphology in a computer model of atrial fibrillation. *J Cardiovasc Electrophysiol*. 2003;14:S172-179
8. Seemann G, Hoper C, Sachse FB, Dossel O, Holden AV, Zhang H. Heterogeneous three-dimensional anatomical and electrophysiological model of human atria. *Philos Transact A Math Phys Eng Sci*. 2006;364:1465-1481
9. Aslanidi OV, Colman MA, Stott J, Dobrzynski H, Boyett MR, Holden AV, Zhang H. 3d virtual human atria: A computational platform for studying clinical atrial fibrillation. *Prog Biophys Mol Biol*.107:156-168
10. Harrild DM, Henriquez CS. A computer model of normal conduction in the human atria. *Circulation Research*. 2000;87:E25-E36
11. Cherry EM, Fenton FH. Visualization of spiral and scroll waves in simulated and experimental cardiac tissue. *New Journal of Physics*. 2008;10
12. Kneller J, Zou RQ, Vigmond EJ, Wang ZG, Leon LJ, Nattel S. Cholinergic atrial fibrillation in a computer model of a two-dimensional sheet of canine atrial cells with realistic ionic properties. *Circulation Research*. 2002;90:E73-E87
13. Jacquemet V, Virag N, Ihara Z, Dang L, Blanc O, Zozor S, Vesin JM, Kappenberger L, Henriquez C. Study of unipolar electrogram morphology in a computer model of atrial fibrillation. *Journal of Cardiovascular Electrophysiology*. 2003;14:S172-S179
14. Courtemanche M, Ramirez RJ, Nattel S. Ionic targets for drug therapy and atrial fibrillation-induced electrical remodeling: Insights from a mathematical model. *Cardiovascular research*. 1999;42:477-489
15. Courtemanche M, Ramirez RJ, Nattel S. Ionic targets for drug therapy and atrial fibrillation-induced electrical remodeling: Insights from a mathematical model. *Cardiovasc Res*. 1999;42:477-489

16. Van Wagoner DR, Pond AL, Lamorgese M, Rossie SS, McCarthy PM, Nerbonne JM. Atrial l-type ca2+ currents and human atrial fibrillation. *Circ Res*. 1999;85:428-436
17. Li GR, Eng JL, Wang ZG, Fermini B, Nattel S. Adrenergic modulation of ultrarapid delayed rectifier k+ current in human atrial myocytes. *Circulation Research*. 1996;78:903-915
18. Kathofer S, Zhang W, Karle C, Thomas D, Schoels W, Kiehn J. Functional coupling of human beta(3)-adrenoreceptors to the kvlqt1/mink potassium channel. *Journal of Biological Chemistry*. 2000;275:26743-26747
19. Heath BM, Terrar DA. Protein kinase c enhances the rapidly activating delayed rectifier potassium current, ikr, through a reduction in c-type inactivation in guinea-pig ventricular myocytes. *J Physiol*. 2000;522 Pt 3:391-402
20. Thomas D, Kiehn J, Katus HA, Karle CA. Adrenergic regulation of the rapid component of the cardiac delayed rectifier potassium current, i-kr, and the underlying herg ion channel. *Basic Research in Cardiology*. 2004;99:279-287
21. Mazhari R, Greenstein JL, Winslow RL, Marban E, Nuss HB. Molecular interactions between two long-qt syndrome gene products, herg and kcne2, rationalized by in vitro and in silico analysis. *Circ Res*. 2001;89:33-38
22. Tanskanen AJ, Greenstein JL, O'Rourke B, Winslow RL. The role of stochastic and modal gating of cardiac l-type ca2+ channels on early after-depolarizations. *Biophys J*. 2005;88:85-95
23. Song Y, Xia Y, Gong KZ, Xu M, Zhang YY, Guo JH, Zhang P. Regulation of gap-junction protein connexin 43 by beta-adrenergic receptor stimulation in rat cardiomyocytes. *Acta Pharmacologica Sinica*. 2009;30:928-934
24. Lowenstein WR. Regulation of cell-to-cell communication by phosphorylation. *Biochem Soc Symp*. 1985;50:43-58
25. Visentin S, Wu SN, Belardinelli L. Adenosine-induced changes in atrial action-potential - contribution of ca and k currents. *American Journal of Physiology*. 1990;258:H1070-H1078
26. Kunze DL. Rate-dependent changes in extracellular potassium in the rabbit atrium. *Circulation research*. 1977;41:122-127
27. Miyata A, Dowell JD, Zipes DP, Rubart M. Rate-dependent [k+](o) accumulation in canine right atria in vivo: Electrophysiological consequences. *American journal of physiology. Heart and circulatory physiology*. 2002;283:H506-517
28. Attwell D, Cohen I, Eisner DA. The effects of heart-rate on the action-potential of guinea-pig and human ventricular muscle. *Journal of Physiology-London*. 1981;313:439-461